Microscopic Evolution of Nuclear Equilibrium Shapes

Tamara Nikšić [a] & Dario Vretenar [a]

[a] Physics Department, University of Zagreb, Zagreb, Croatia

Available online: 05 Dec 2011

PLEASE SCROLL DOWN FOR ARTICLE

Microscopic Evolution of Nuclear Equilibrium Shapes

Tamara Nikšić and Dario Vretenar
Physics Department, University of Zagreb, Zagreb, Croatia

Introduction

The rich variety of nuclear shapes has been the subject of extensive experimental and theoretical studies. The variation of ground-state shapes in an isotopic chain, for instance, is governed by the evolution of the shell structure of single-nucleon orbitals. Far from the β-stability line, in particular, the energy spacings between single-nucleon levels change considerably with the number of neutrons and/or protons. This can result in reduced spherical shell gaps, modifications of shell structure, and in some cases spherical magic numbers may disappear. The reduction of spherical shell closure is often associated with the occurrence of deformed ground states and, in a number of cases, with the phenomenon of coexistence of different shapes in a single nucleus.

In most cases the transition between different shapes in isotopic or isotonic sequences is gradual, and reflects the underlying modifications of single-nucleon shell-structure and the interactions between valence nucleons. In a number of examples, however, with the addition or subtraction of only few nucleons one finds signatures of abrupt changes in observables that characterize ground-state nuclear shapes. In the last decade the concept of quantum phase transitions has successfully been applied and investigated, both experimentally and theoretically, in studies of equilibrium shape changes of nuclei. The understanding and quantitative description of the evolution of nuclear shapes, including regions of short-lived exotic nuclei that are becoming accessible in experiments at radioactive-beam facilities, necessitate accurate modeling of the underlying microscopic nucleonic dynamics. Major advances in nuclear theory have recently been made in studies of complex shapes and the corresponding excitation spectra and electromagnetic decay patterns, especially in the framework of nuclear density functionals.

Nuclear Energy Density Functionals

Ab initio methods, starting from a microscopic Hamiltonian that accurately reproduces nucleon-nucleon scattering and few-body data, have been very successful in the description of light nuclei up to oxygen isotopes, and large-scale semi-microscopic shell-model calculations can be performed for medium-heavy and even some heavy nuclei in the vicinity of closed shells. However, the only comprehensive approach to nuclear structure is presently based on the framework of energy density functionals (EDFs). Nuclear EDFs enable a complete and accurate description of ground-state properties and collective excitations over the whole nuclide chart. No other method achieves comparable global accuracy at the same computational cost, and it is the only one that can describe the evolution of structure phenomena from relatively light systems to super-heavy nuclei, and from the valley of β-stability to the particle drip-lines [1–3].

In practical implementations nuclear EDFs are analogous to Kohn-Sham density functional theory (DFT) [4, 5], the most widely used method for electronic structure calculations in condensed matter physics and quantum chemistry. In DFT a quantum many-body system is described in terms of a universal energy density functional that, for a given inter-particle interaction, has the same functional form for all systems.

The ground-state energy and density of a given system can be determined by minimizing an EDF with respect to the 3-dimensional density. The self-consistent Kohn-Sham scheme introduces a local effective single-particle potential, such that the exact ground-state density of the interacting system of particles equals the ground-state density of the auxiliary non-interacting system, expressed in terms of the lowest occupied single-particle orbitals—solutions of the Kohn-Sham equations. Kohn-Sham DFT provides accurate predictions for atoms, molecules, nanostructures, solids, and solid surfaces. In the nuclear case the many-body dynamics is represented by independent nucleons moving in a local self-consistent mean-field potential that correspond to the actual density and current distributions of a given nucleus.

The unknown exact nuclear EDF is approximated by relatively simple functionals of powers and gradients of ground-state nucleon densities and currents, representing distributions of matter, spins, momentum, and kinetic energy. Both relativistic and non-relativistic realizations of

EDFs are employed in studies of nuclear matter and finite nuclei. In principle a nuclear EDF can incorporate all short-range correlations related to the repulsive core of the inter-nucleon interaction, and long-range correlations mediated by nuclear resonance modes. An additional functional of the pairing density is included to account for effects of superfluidity in open-shell nuclei.

Even though it originates in the effective interaction between nucleons, a generic density functional is not necessarily related to any given nucleon-nucleon potential and, in fact, some of the most successful modern functionals are entirely empirical. Of course it would be desirable to have a fully microscopic foundation for a universal density functional, and this is certainly one of the major challenges for the framework of nuclear EDFs [6]. However, even if a fully microscopic EDF is eventually developed, the parameters of that functional will still have to be fine-tuned to structure data of finite nuclei. This is because data on nucleon-nucleon scattering and few-nucleon systems, or bulk properties of infinite nuclear matter, cannot determine the density functional to a level of accuracy necessary for a quantitative description of medium-heavy and heavy nuclei. Until recently the standard procedure of fine-tuning global nuclear density functionals was to perform a *least-squares* adjustment of a small set of free parameters simultaneously to empirical properties of symmetric and asymmetric nuclear matter, and to selected ground-state data of about ten spherical closed-shell nuclei. A new generation of semi-microscopic and fully microscopic functionals is currently being developed that will, on the one hand, establish a link with the underlying theory of strong interactions—low-energy QCD and, on the other hand, provide accurate predictions for a wealth of new data on short-lived nuclei far from stability that are produced at radioactive-beam facilities. To obtain unique parameterizations, these functionals will have to be adjusted to a larger data set of ground-state properties, including both spherical and deformed nuclei [6–8].

To illustrate the universality of the EDF approach to nuclear structure, all examples presented in this article have been calculated using a single functional—the relativistic functional DD-PC1 [7]. Starting from microscopic nucleon self-energies in nuclear matter, and empirical global properties of the nuclear matter equation of state, the coupling parameters of DD-PC1 were fine-tuned to the experimental masses of a set of 64 deformed nuclei in the mass regions $A \approx 150$–180 and $A \approx 230$–250. The functional has been further tested in calculations of medium-heavy and heavy nuclei, including binding energies, charge radii, deformation parameters, neutron skin thickness, and excitation energies of giant multipole resonances. For the examples considered here, pairing correlations have been taken into account by employing an interaction that is separable in momentum space, and is completely determined by two parameters adjusted to reproduce the empirical bell-shaped pairing gap in symmetric nuclear matter [9].

The advantages of using EDFs in the description of nuclear structure phenomena are evident already at the basic level of implementation: an intuitive interpretation of mean-field results in terms of intrinsic shapes and single-particle states, calculations performed in the full model space of occupied states (no distinction between core and valence nucleons, no need for effective charges), and the universality of EDFs that enables their applications to *all* nuclei throughout the periodic chart. The latter feature is especially important for extrapolations to regions of exotic short-lived nuclei far from stability for which few, if any, data are available.

The Kohn-Sham equations (Schrödinger-like for non-relativistic functionals, or Dirac-like for relativistic EDFs, with the Hamiltonian defined as the functional derivative of the EDF with respect to density) are solved in the intrinsic frame of reference attached to the nucleus, in which the shape of the nucleus can be arbitrarily deformed. The simplest case corresponds to five-dimensional quadrupole dynamics. Figure 1 displays the self-consistent quadrupole binding-energy maps of the even-even isotopes $^{72–78}$Kr in the β–γ plane, calculated with the relativistic Hartree-Bogoliubov (RHB) model [3]. The map of the energy surface as function of quadrupole deformation is obtained by imposing constraints on the axial and triaxial mass quadrupole moments. The moments can be related to the polar deformation parameters β and γ. The parameter β is simply proportional to the intrinsic quadrupole moment, and the angular variable γ specifies the type and orientation of the shape. The limit $\gamma = 0°$ corresponds to axial prolate shapes, whereas the shape is oblate for $\gamma = 60°$. Triaxial shapes are associated with intermediate values $0° < \gamma < 60°$. For each surface shown in Figure 1, all energies are normalized with respect to the binding energy of the absolute minimum, and the color code refers to the energy of each point on the surface relative to the minimum.

Neutron-deficient nuclei in the mass region $A \approx 70$–80 are predicted to display coexisting prolate and oblate shapes, as a result of competing large shell gaps for both
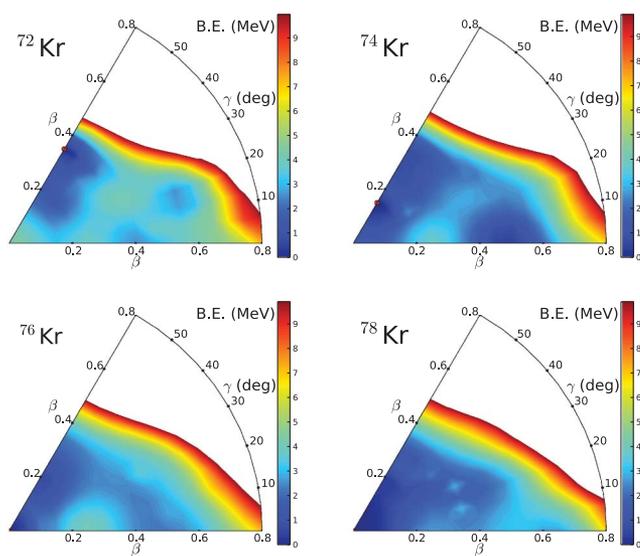
Figure 1. *Self-consistent binding-energy maps of the even-even isotopes $^{72-78}$Kr in the β–γ plane ($0° \leq \gamma \leq 60°$).*

types of deformations at proton/neutron numbers 34, 36, and 38. The calculated maps indicate that the four Kr isotopes are rather soft with respect to both β and γ degrees of freedom. The occurrence of nearly degenerate minima raises the question of their stability against dynamical effects of collective correlations [10].

Collective Correlations

Maps of the energy surface as function of quadrupole deformation nicely illustrate the variation of ground-state shapes governed by the evolution of shell structure, but they are not observables and cannot directly be compared to data. A static self-consistent mean-field solution of the nuclear Kohn-Sham equations in the intrinsic frame is characterized by symmetry breaking—translational, rotational, particle number, and can only provide an approximate description of bulk ground-state properties such as masses and radii. When considering applications, an important challenge for the framework of EDF is the systematic treatment of dynamical effects related to restoration of broken symmetries and fluctuations in collective coordinates. To calculate excitation spectra and transition rates, it is necessary to project from the mean-field solution states with good quantum numbers—angular momentum, particle number, and also take into account fluctuations around the mean-field minimum. The corresponding

correlation energy, that is, the energy gained by symmetry restoration and quantum fluctuations, can reach several MeV for a well-deformed configuration.

Collective correlations are sensitive to shell effects, display pronounced variations with particle number and, therefore, cannot *a priori* be incorporated in a universal EDF. The Kohn-Sham EDF framework has to be extended to take into account collective correlations. Symmetry restoration and fluctuations of quadrupole deformation can be treated simultaneously by mixing angular-momentum and particle-number projected states that correspond to different intrinsic configurations. The most effective approach for configuration mixing calculations is the generator coordinate method (GCM), with multipole moments used as coordinates that generate the intrinsic wave functions. When used on top of the self-consistent mean-field solution in the intrinsic frame, this method provides an *a posteriori* treatment of collective correlations.

In recent years several accurate and efficient models, based on microscopic energy density functionals, have been developed that perform restoration of symmetries broken by the static nuclear mean field, and take into account quadrupole fluctuations. Many interesting phenomena related to shell evolution have been investigated by employing the angular-momentum and particle-number projected GCM with the axial quadrupole moment as the generating coordinate, and with intrinsic configurations based on non-relativistic or relativistic EDFs. However, while GCM configuration mixing of axially symmetric states has routinely been employed in structure studies, the application of this method to triaxial shapes presents a much more involved and technically difficult problem. Only the most recent advances in parallel computing and modeling have enabled the implementation of microscopic models, based on triaxial symmetry-breaking intrinsic states that are projected on particle number and angular momentum, and finally mixed by the generator coordinate method. Applications to heavy nuclei, however, are still computationally very demanding and time-consuming [11–13].

In an approximation to the full GCM approach to five-dimensional quadrupole dynamics, a collective Hamiltonian can be formulated that restores rotational symmetry and accounts for fluctuations around the triaxial mean-field minima. The dynamics of the five-dimensional Hamiltonian for quadrupole vibrational and rotational degrees of freedom is governed by the seven functions of the intrinsic deformations β and γ: the collective potential, the three

vibrational mass parameters: $B_{\beta\beta}$, $B_{\beta\gamma}$, $B_{\gamma\gamma}$, and three moments of inertia for rotations around the principal axes [14–16]. These functions are determined by constrained microscopic mean-field calculations using a given nuclear EDF. Starting from self-consistent Kohn-Sham orbitals, the corresponding occupation probabilities and energies at each point on the energy surfaces shown in Figure 1, the mass parameters and the moments of inertia are calculated as functions of the deformations β and γ. The diagonalization of the resulting Hamiltonian yields excitation energies and collective wave functions that can be used to calculate various observables, such as electromagnetic transition rates.

In Figure 2 we plot the corresponding low-energy spectrum of collective states of ^{74}Kr in comparison with available data [10]. The calculated spectrum is in very good agreement with experiment, not only for the ground-state band (yrast states) but also for structures above the yrast. The collective states are completely determined by the DD-PC1 energy density functional plus a separable pairing interaction, and the transition probabilities are calculated in the full configuration space using the bare value of the proton charge [17]. The structure of low-lying states in the neutron-deficient krypton isotopes is characterized by the coexistence of different shapes. For ^{74}Kr, in particular, the two lowest 0^+ states exhibit a pronounced mixing of oblate and prolate configurations. This mixing can be attributed to the softness of the potential with respect to the γ-deformation parameter. Even though the ground state is not prolate,

the collective functions of the other yrast states are concentrated close to the $\gamma = 0°$ axis, and the prolate character of these states is also reflected in the calculated spectroscopic moments, in good agreement with the experimental values.

Shape Phase Transitions

Phase transitions in equilibrium nuclear shapes correspond to first- and second-order quantum phase transitions (QPT) induced by variation of a non-thermal control parameter (number of nucleons) at zero temperature [18–20]. Theoretical studies have typically been based on phenomenological geometric models of nuclear shapes and potentials, or algebraic models of nuclear structure, but recently several microscopic analyses of shape QPT have been reported, that start from nucleonic degrees of freedom. A phase transition is characterized by a significant variation of one or more order parameters as functions of the control parameter. Even though in systems composed of a finite number of particles phase transitions are actually smoothed out, in many cases clear signatures of abrupt changes of structure properties are observed. There are basically two approaches to study QPT: first, the method of Landau, based on potentials and, second, the direct computation of order parameters. In the case of atomic nuclei, however, a quantitative analysis of QPT must go beyond a simple study of potential energy surfaces. This is because potentials or, more specifically, deformation parameters that characterize potential energy surfaces, are not observables, and can only be related to observables by making very specific model assumptions. Both approaches can be combined in a consistent microscopic framework, based on nuclear EDFs, that can be used for calculation of observables related to quantum order parameters [21–23]. An order parameter is a measure of the degree of order in a system. As a normalized quantity that is zero in one (symmetric) phase, and non-zero in the other, it characterizes the onset of order at the phase transition [24].

The two most studied classes of nuclear shape phase transitions, both theoretically and experimentally, correspond to a second-order QPT between spherical and γ-soft shapes, and a first-order QPT between spherical and axially-deformed shapes. The former is a phase transition in one degree of freedom—the axial deformation β. The critical point of phase transition can also be related to a dynamical symmetry: in this case E(5) [25], and the experimental realization of this critical-point symmetry was first identified in the spectrum of ^{134}Ba [26]. The second type of shape transitions, between spherical and axially deformed
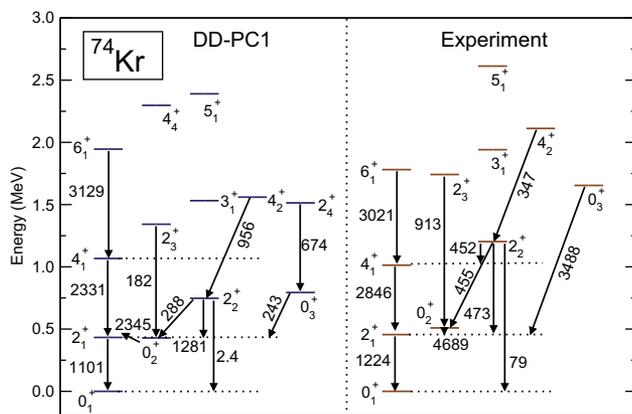

Figure 2. *The low energy spectrum of ^{74}Kr calculated with the DD-PC1 relativistic density functional (left) compared to data (right) for the excitation energies and intraband and interband B(E2) values (in e^2 fm^4).*

nuclei, is more commonly encountered and involves two degrees of freedom—the deformations β and γ. The critical point of this phase transition, denoted X(5) [27], does not correspond to a dynamical symmetry in the usual sense. Nevertheless, for the particular case in which the β and γ degrees of freedom are decoupled, an approximate analytic solution at the critical point of phase transition can be expressed in terms of zeros of Bessel functions of irrational order. Evidence for the empirical realization of X(5) phase transition was first reported for ^{152}Sm and other N = 90 isotones [28]. ^{150}Nd, in particular, is considered to be a good example of empirical realization of the X(5) model for the critical point of phase transition [29].

In Figure 3 we plot the RHB quadrupole binding-energy maps of the transitional even-even nuclei ^{148,150,152}Nd, calculated using the functional DD-PC1. These plots illustrate the increase of prolate deformation with the number of neutrons, from spherical shapes in the region near the neutron shell N = 82 (not shown in the figure), to the strongly deformed ^{154}Nd. The deformed Nd isotopes display prolate minima, and a pronounced feature of shape evolution is the broad flat minimum in ^{150}Nd, that extends in the interval 0.2 ≤ β ≤ 0.4. In this region the potential displays a parabolic dependence on γ for γ ≤ 30°, and then flattens out towards the oblate axis. The flat bottom of a potential has been considered a signature of possible shape phase transition because it allows for fluctuations of collective variables. The self-consistent single-nucleon states that correspond to each point on the energy surface are used to calculate the parameters that determine the collective Hamiltonian, yielding the excitation energies and collective wave functions. For all three Nd nuclei the spectra and transition probabilities reproduce available data and, for ^{150}Nd in particular, the low-energy spectrum is in excellent agreement with the predictions of the X(5) model for the critical point of first-order phase transition.

Signatures of phase transitions characterize the evolution of both excitation spectra and order parameters. To verify that the collective Hamiltonian based on the functional DD-PC1 predicts the shape phase transition precisely at the isotope ^{150}Nd, we also need to consider the neighboring nuclei ^{148}Nd and ^{152}Nd. This is illustrated in the two upper panels of Figure 4 where, for the yrast states of these three isotopes, we compare the B(E2; L → L-2) values and excitation energies calculated using the collective Hamiltonian, with the corresponding values predicted by the X(5) model, and with the limit of axially-deformed rigid rotor. Obviously the E2 rates and excitation

energies for ^{150}Nd are closest to those calculated from analytic expressions corresponding to the X(5) model for the phase-transitional point. ^{148}Nd does not differ very much from the X(5) limit, whereas the yrast states of ^{152}Nd indicate that this nucleus is already closer to a deformed rotor.
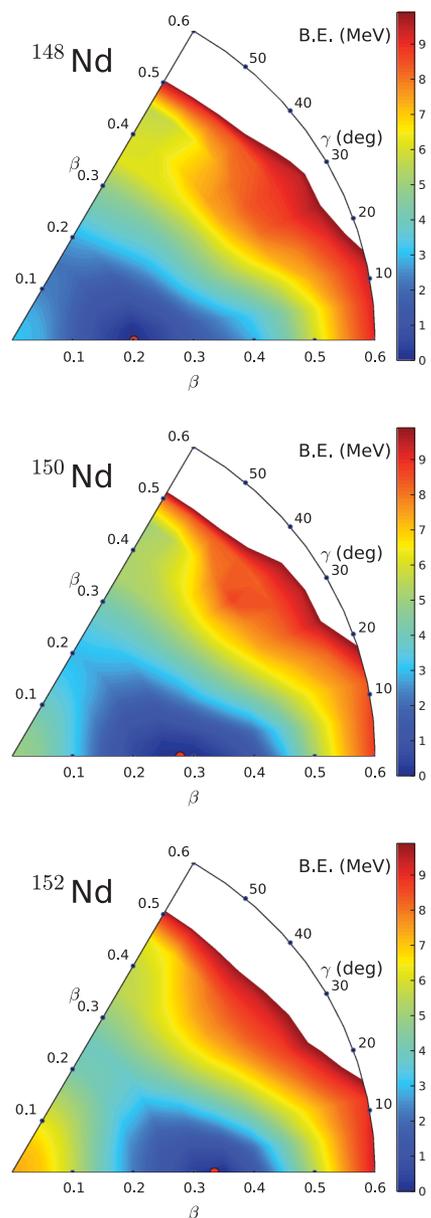

Figure 3. *Self-consistent binding-energy maps of ^{148,150,152}Nd in the β–γ plane (0° ≤ γ ≤ 60°).*

We emphasize, however, that the physical control parameter – the nucleon number, is not continuous and thus in general a microscopic calculation cannot exactly reproduce the point of QPT.

In the lowest panel of Figure 4 we analyze an example of calculation of observables that can be related to order parameters. The phase transition is between coexisting different shapes in the two lowest 0^+ states: the ground state 0_1^+ and the excited state 0_2^+. It can be quantified in terms of a model-independent quadrupole shape invariant. For the n-th 0^+ state, the invariant $q_2(0_n^+)$ is defined by the relation:

$$q_2(0_n^+) = \sum_{j=1}^{\infty} B(E2; 0_n^+ \to 2_j^+) \sim \beta_{eff}^2(0_n^+).$$

It is proportional to the square of the effective β-deformation of the state 0_n^+. In principle, transitions from this state to all 2^+ states are included in the sum but in practice a truncated sum suffices [30]. For the lowest 0^+ states a good approximation can already be obtained by truncating the sum to transitions to the first three or four lowest 2^+ states. In most cases, of course, data on B(E2) values will only be available for a few lowest 2^+ states. Figure 4 shows the quadrupole shape invariants q_2 of the ground state 0_1^+ and the excited state 0_2^+ as functions of the neutron number. $k = 4$ means that transitions to the four lowest 2^+ states have been included in the sum over B(E2) values. A very interesting result of this calculation is that the two shape invariants cross precisely between ^{150}Nd and ^{152}Nd. On the right hand side of the lowest panel in Figure 4 we also plot the difference between the two shape invariants, and this quantity clearly reflects the phase transition to the axially-deformed rotational nucleus ^{152}Nd. As a function of the control parameter (number of neutrons), this difference displays a behavior that is characteristic for a first-order transition. Even though the calculation has been carried out for a finite number of paricles, the phase transition does not appear to be significantly smoothed out by the finiteness of the nuclear system.

Evolution of Non-Axial Shapes in Pt Isotopes

Most deformed nuclei display axially symmetric prolate ground-state shapes, but few areas of the nuclide chart are characterized by the occurrence of non-axial shapes. One example is the A ≈ 190 mass region, where both prolate to oblate shape transitions, and even triaxial ground-state shapes have been predicted. Figure 5 shows the self-consistent RHB quadrupole binding energy maps of the even-A $^{190-196}Pt$ isotopes in the $\beta - \gamma$ plane, calculated with the DD-PC1 energy density functional. The energy surfaces are γ-soft, with shallow minima at γ ≈ 30°. In general the equilibrium deformation decreases with mass number and, proceeding to even heavier isotopes, one finds that the energy map of ^{198}Pt has also a non-axial minimum,
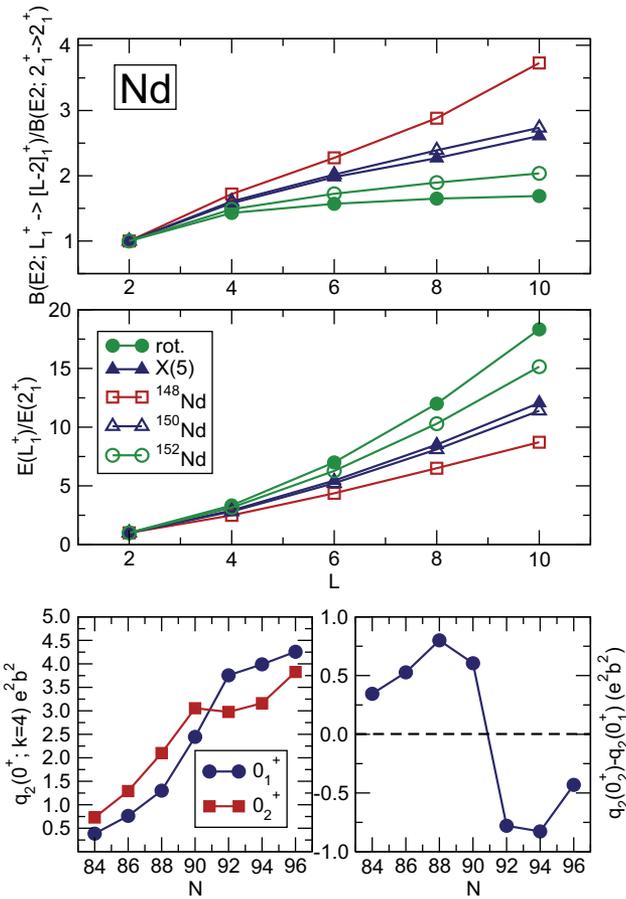

Figure 4. *B(E2; L → L-2) values (upper panel) and excitation energies (middle panel) for the yrast states of ^{148}Nd, ^{150}Nd, and ^{152}Nd, calculated with the collective Hamiltonian based on the functional DD-PC1 and compared to those predicted by the X(5) model for the phase-transitional point, and by the axially deformed rotor model. Evolution of the shape invariants q_2 for the first two 0^+ states, as functions of neutron number in Nd isotopes (lower panel).*
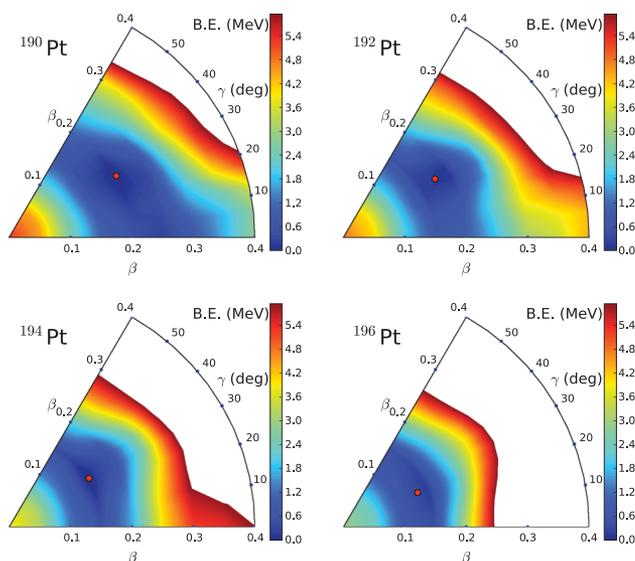
Figure 5. *Self-consistent binding-energy maps of the even-even isotopes $^{190-196}$Pt in the $\beta - \gamma$ plane ($0 \le \gamma \le 60°$).*

whereas ^{200}Pt displays a slightly oblate minimum, signaling the shell-closure at the neutron number N = 126.

The formation of deformed triaxial minima can be related to the occurrence of gaps or regions of low single-particle level density around the Fermi surface at $\gamma \approx 30°$, and this is reflected in the low excitation energies of the γ-vibrational bands. As an example, in the upper panel of Figure 6 we plot the neutron single-particle levels of ^{192}Pt as functions of the deformation parameters along a closed path in the $\beta - \gamma$ plane. Solid curves correspond to levels with positive parity, and short-dashed curves denote levels with negative parity. The long-dashed (yellow) curve corresponds to the Fermi level. The panels on the left and right display prolate ($\gamma = 0°$) and oblate ($\gamma = 60°$) axially-symmetric single-neutron levels, respectively. In the middle panel the single-neutron levels are plotted as functions of γ for a fixed value of the axial deformation $\beta = 0.175$, at the position of the equilibrium minimum of the binding energy surface (Figure 5). The formation of a gap between the neutron single-particle levels in the vicinity of the Fermi surface around $\gamma \approx 30°$ is clearly seen in this diagram, and a similar effect is found in the plot of proton single-particle levels. The corresponding low-energy spectrum of ^{192}Pt, obtained from the collective Hamiltonian, is shown in the lower panel of Figure 6. The calculated ground-state and

γ-vibration bands are compared to the corresponding sequences of experimental states [31]. Both the theoretical excitation energies and B(E2) values are in agreement with data. In particular, one might notice the excellent result for the predicted excitation energy of the band-head of the γ-band, as well as the good agreement with the experimental B(E2) values for transitions between the γ-band and the yrast band. This result indicates that the DD-PC1 potential has the correct stiffness with respect to the γ-degree of freedom. A similar quantitative agreement with data is also obtained in the calculation of low-energy spectra for the
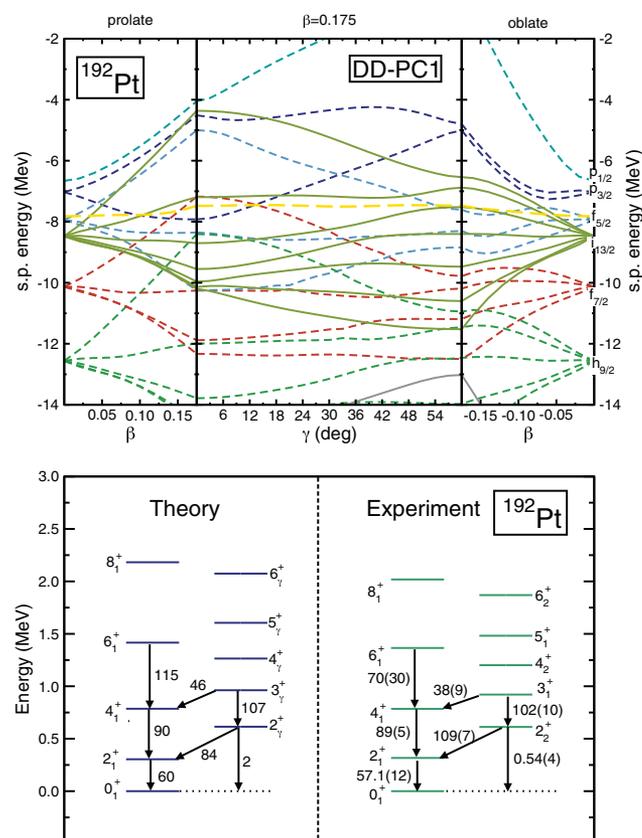

Figure 6. *Neutron single-particle levels in ^{192}Pt as functions of the quadrupole deformation parameters β and γ (upper panel; see text for description). In the lower panel the resulting collective low-energy spectrum (left) is compared with the to data (right) for the excitation energies and, intraband and interband B(E2) values (in Weisskopf units).*

other Pt isotopes for which the energy maps are shown in Figure 5.

Conclusions

Structure phenomena related to shape evolution in atomic nuclei continue to be a very active research topic in low-energy nuclear physics. Dedicated radioactive-beam facilities, in particular, provide new and intriguing data on shapes in regions of exotic nuclei far from stability. Key questions addressed by experimental programs also require developing advanced theoretical methods. It is important to formulate and implement microscopic models, based on the underlying dynamics of low-energy strong interactions, that can be employed to quantitatively describe the rich variety of shape phenomena, and the resulting complex excitation spectra and decay patterns across the entire chart of nuclides. Such a framework is provided by nuclear energy density functionals (NEDFs). By employing a single EDF, parameterized with a small set of universal constants, in this article we have presented a quantitative analysis of shape coexistence in neutron-deficient Kr isotopes, a ground-state shape phase transition in $N \approx 90$ Nd nuclei, and the appearance of triaxial shapes in Pt isotopes. The description of these apparently diverse phenomena in a single microscopic framework, the interpretation of complex spectra in terms of shapes and the underlying evolution of shell structures, and the quantitative agreement with data, illustrate the universality of the EDF approach to nuclear structure.

Acknowledgments

References

1. G. A. Lalazissis, P. Ring, and D. Vretenar (Eds.), *Extended Density Functionals in Nuclear Structure Physics, Lecture Notes in Physics 641, (Springer, Heidelberg, 2004).*
2. M. Bender, P.-H. Heenen, and P.-G. Reinhard, *Rev. Mod. Phys*. 75 (2003) 121.
3. D. Vretenar, A. V. Afanasjev, G. A. Lalazissis, and P. Ring, *Phys. Rep*.409 (2005) 101.
4. W. Kohn, *Rev. Mod. Phys*. 71 (1999) 1253.
5. R. M. Dreizler and E. K. U. Gross, *Density Functional Theory (Springer, Berlin, 1990).*
6. J. E. Drut, R. J. Furnstahl, and L. Platter, *Prog. Part. Nucl. Phys*. 64 (2010) 120.
7. T. Nikšić, D. Vretenar, and P. Ring, *Phys. Rev*. C 78 (2008) 034318.
8. M. Kortelainen, T. Lesinski, J. More, W. Nazarewicz, J. Sarich, N. Schunck, M. V. Stoitsov, and S. Wild, *Phys. Rev*. C 82 (2010) 024313.
9. T. Nikšić, P. Ring, D. Vretenar, Y. Tian, and Z. Y. Ma, *Phys. Rev*. C 81 (2010) 054318.
10. E. Clement et al., *Phys. Rev*. C 75 (2007) 054313.
11. M. Bender and P.-H. Heenen, *Phys. Rev*. C 78 (2008) 024309.
12. T. R. Rodriguez and J. L. Egido, *Phys. Rev*. C 81 (2010).
13. J. M. Yao, J. Meng, P. Ring, and D. Vretenar, *Phys. Rev*. C 81 (2010), 044311.
14. P.-G. Reinhard and K. Goeke, *Rep. Prog. Phys*. 50 (1987) 1.
15. L. Prochniak and S. G. Rohozinski, *J. Phys*. G 36 (2009) 123101.
16. T. Nikšić, Z. P. Li, D. Vretenar, L. Prochniak, J. Meng, and P. Ring, *Phys. Rev*. C 79 (2009) 034303.
17. T. Nikšić, D. Vretenar, and P. Ring, *Prog. Part. Nucl. Phys*. 46 (2011) 519.
18. F. Iachello, in Proceedings of the *International School of Physics "Enrico Fermi" Course CLIII*, A. Molinari, L. Riccati, W. M. Alberico and M. Morando (Eds.) IOS Press, Amsterdam 2003.
19. R. F. Casten and E. A. McCutchan, *J. Phys. G: Nucl. Part. Phys*. 34 (2007) R285.
20. P. Cejnar, J. Jolie, and R. F. Casten, *Rev. Mod. Phys*. 82 (2010) 2155.
21. T. Nikšić, D. Vretenar, G. A. Lalazissis, and P. Ring, *Phys. Rev. Lett*. 99 (2007) 092502.
22. Z. P. Li, T. Nikšić, D. Vretenar, J. Meng, G. A. Lalazissis, and P. Ring, *Phys. Rev*. C 79 (2009) 054301.
23. Z. P. Li, T. Nikšić, D. Vretenar, and J. Meng, *Phys. Rev*. C 81 (2010) 034316.
24. Z. P. Li, T. Nikšić, D. Vretenar, and J. Meng, *Phys. Rev*. C 80 (2009) 061301.
25. F. Iachello, *Phys. Rev. Lett*. 85 (2000) 3580.
26. R. F. Casten and N. V. Zamfir, *Phys. Rev. Lett*. 85 (2000) 3584.
27. F. Iachello, *Phys. Rev. Lett*. 87 (2001) 052502.
28. R. F. Casten and N. V. Zamfir, *Phys. Rev. Lett*. 87 (2001) 052503.
29. R. Kruecken et al., *Phys. Rev. Lett*. 88 (2002) 232501.
30. V. Werner, E. Williams, R. J. Casperson, R. F. Casten, C. Scholl, and P. von Brentano, *Phys. Rev*. C 78 (2008) 051303(R).
31. Coral M. Baglin, *Nuclear Data Sheets* 84 (1998) 717.